Design of a hydrogen/tritium permeation sensor for Gen-IV sodium fast reactors

Design of a Hydrogen/Tritium Permeation Sensor for Gen-IV Sodium Fast Reactors

L. Candido[a,*], C. Alberghi[a], M. Utili[b]

[a] *ESSENTIAL Group, Politecnico di Torino - Corso Duca degli Abruzzi, 24, 10129, Torino, Italy*
[b] *ENEA C.R. Brasimone – Località Brasimone, 40043 Camugnano (BO), Italy*

Abstract

A crucial issue for the design of a fission Generation IV Sodium Fast Reactor (SFR) is to efficiently characterise the processes and the technical solutions devoted to the management and the control of tritium transfers and releases occurring in SFR circuits. In fact, the tritium balance in sodium fast reactor is a key aspect and the determination of the hydrogen isotopes (hydrogen/tritium) concentration in the liquid sodium has to be investigated for the operational control of tritium balance in the reactor. Therefore, the need for a fast and reliable sensor for the online measurement of hydrogen isotopes concentration in sodium is evident. In the present work, a new concept of hydrogen isotopes permeation sensor (HPS) is shown. The physical operating principle of the HPS is the permeation of hydrogen isotopes throughout a thin metallic membrane. Since the limit of detection and the accuracy of the integrated sensor has to be compatible with the range of tritium concentrations in sodium circuits, it is necessary for the sensor to be operated in high vacuum (HV) conditions in order to guarantee hydrogen isotopes measurements down to 10^{-5} Pa or even lower. The paper presents two designs foreseen not only for SFRs, but also for an experimental sodium loop where higher H_2 concentrations will be adopted.

Keywords: SFR, tritium, permeation sensors, HV

1. Introduction

In liquid metals contained in nuclear reactors, the partial pressure of hydrogen isotopes, hereafter indicated as Q (Q=H, D, T), historically has been measured in the liquid metal using off-line processes [1]. However, a better solution is to use an in-process, near real time technology able to track the tritium production. Such technology has been developed for fusion applications during the years by ENEA C. R. Brasimone, in collaboration with Politecnico di Torino [2, 3, 4], showing a high accuracy in the detection of Q concentration in flowing liquid LiPb. Preliminary evaluations of the accuracy showed it varies from 3 to 7% [5]. Starting from this know-how, the development of a sodium Q meter for Generation-IV sodium fast breeder fission reactors (SFRs) is planned by using a similar conceptual approach adopted for sensors development for LiPb. Permeation sensors are one of the most promising technological candidates for hydrogen isotopes measurements [6] in liquid metals due to their reliability, but this kind of sensors is not able to measure selectively each isotope. Therefore, it is necessary to integrate the sensor with an ionization chamber or a mass spectrometer. Other technologies, such as electrochemical sensors, are promising but at the actual state of the art their accuracy relies on the calibration in the reactor environment, particularly at the reactor operating temperature [7], limiting the temperature range of applicability. It should be mentioned that for the measurement of Q_2 isotopologues in gas phase, the laser Raman technique available in the Tritium Laboratory Karlsruhe (TLK) is used for high-accuracy, continuous monitoring and measurement of hydrogen isotopes [8, 9]. It should be observed that the limit of detection of this technique is 10 Pa [9].

Although operative hydrogen isotopes pressures being representative of ITER and DEMO fusion reactors conditions (10-1000 Pa) were deeply investigated, to date a systematic understanding of the sensor behaviour at lower pressure conditions is still lacking. Within this frame, a special emphasis should be put on the fact that, in contrast to fusion applications, the vacuum requested for the sensor to be operated in fission Gen-IV SFRs is HV (high vacuum), since the hydrogen isotopes pressure range foreseen may vary between 10^{-3} Pa down to 10^{-5} Pa or even lower. This is a strong constraint for the design, since all the components need to be accurately dimensioned and not only the materials need to be HV-compatible, but also the operative procedures need to be carefully assessed.

In order to perform a design of the hydrogen isotopes permeation sensor (HPS) for sodium applications, a conceptual sodium fast reactor is considered. A general scheme is proposed in Figure 1, along with the possible locations

*Corresponding author
Email address: luigi.candido@polito.it (L. Candido)

for the HPS. The sensors could be installed at the inlet/outlet of the Na/Na heat exchanger, at the inlet/outlet of the intermediate heat exchanger (IHX) and of the steam generator (SG) or Na/gas heat exchanger in the secondary loop. The reactor is composed by three main circuits: a primary sodium loop with the purpose to extract the thermal power from the core, a secondary sodium loop with the aim of reactor safety improving, and a tertiary circuit entering in the power block. The main assumptions on hydrogen isotopes ranges foreseen for the conceptual sodium fast reactor are reported in Table 1.

In SFRs, tritium mostly comes from ternary fission of the fuel and neutron capture reactions inside boron-containing materials, such as control rods and neutron flux shielding blocks. Tritium enters in the primary coolant and then it is circulated or permeated to the secondary coolant throughout the intermediate heat transfer loop. The permeated tritium, subsequently, reacts with the steam/water present in the steam generator through the heat exchanger surfaces. More details on the design of a SFR can be found in [10].

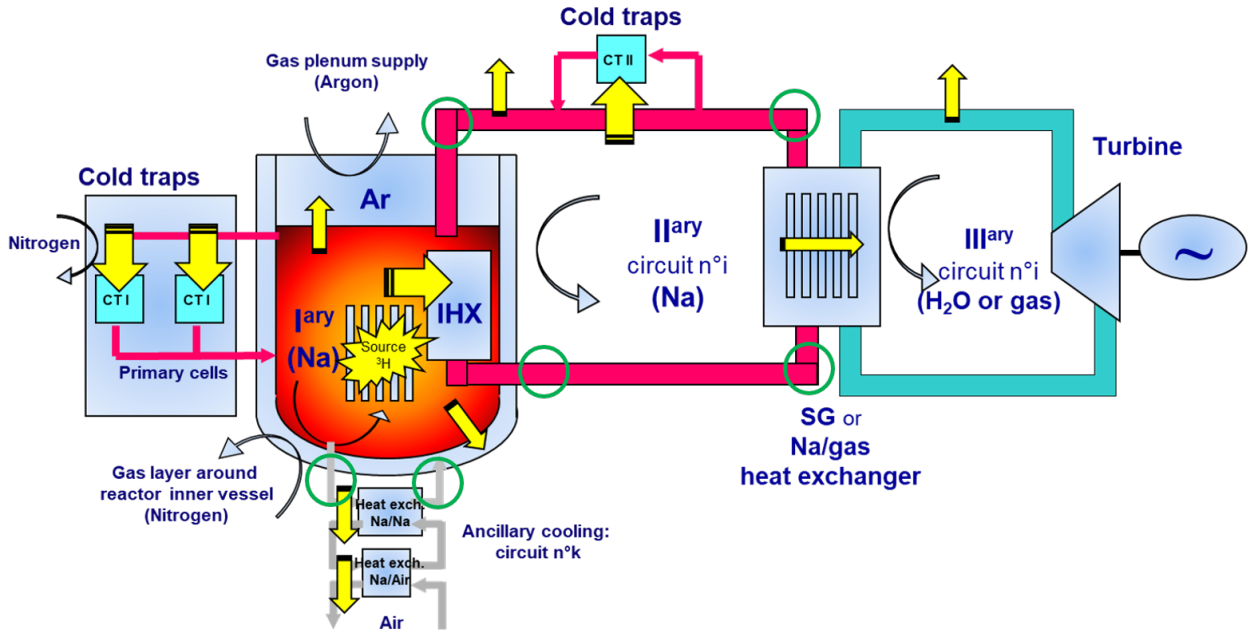

Figure 1: Layout of conceptual sodium fast reactor. Green circles represent the possible locations of HPS.

Hydrogen isotopes solubilized in the liquid sodium are in thermodynamic equilibrium with the hydrogen isotopes partial pressure in the cover gas of the reactor. A mass transfer mechanism is therefore established from the gas phase to the liquid phase, et vice versa, which depends on the mass transfer coefficient, which is still not known. At the moment, parametric studies are being developed in order to quantify more precisely this mechanism, which has a strong impact on the release of gaseous tritium. The maximum release of gaseous tritium (HT) is fixed at 80 TBq/y. Within this frame, a fast sensor able to measure hydrogen isotopes concentration is crucial, since it is necessary to monitor it in the different points of the reactor.

Table 1: Main assumptions on Q_2 isotopes for a conceptual SFR.

Parameter	Values	Units
Operative temperature, T_{op}	400-500	°C
H_2 equilib. partial pressure, p_{H_2}	10^{-3}-10^{-2}	Pa
T_2 equilib. partial pressure, p_{T_2}	10^{-5}-10^{-3}	Pa

In this work, two designs are proposed and investigated. The former is based on a nickel membrane and is developed to be tested in an experimental sodium facility which operates with only hydrogen, at higher partial pressures in the range between 1 and 10 Pa. The latter relies on a tantalum membrane which is foreseen in application to the conceptual sodium fast reactor. Tantalum presents a higher permeability to hydrogen isotopes compared to nickel, but it presents significantly higher costs. The overall structure of this study is hereafter briefly described. Chapter 2 provides an insight of the physics behind hydrogen isotopes permeation sensors and the numerical model developed for its simulation. In Chapter 3, the design of the measuring head is presented, focusing on the material choice and on the numerical outcomes provided by the hydrogen isotopes transport code. The integration in the full sensor line, i.e. the line with all the ancillary components needed for the sensor to work, are detailed in Chapter 4. Within this frame, a discussion on the proposed design focused on the two different applications is given. Finally, Chapter 5 is dedicated to the summary of this work.

2. Theory on hydrogen isotopes permeation sensors

A hydrogen isotopes permeation sensor is composed of a measuring head and a certain set of ancillary systems (hereafter labelled as sensor line) needed for its operation. The measuring head is constituted by a membrane permeable to hydrogen isotopes and immersed in the liquid metal, where hydrogen isotopes are dissolved at a certain concentration in equilibrium with a specific partial pressure. The membrane is connected through a small tube to an external pressure gauge and/or to a vacuum pumping system depending on its mode of operation, the equilibrium mode and the dynamic mode, later discussed. As highlighted in Chapter 1, a mass spectrometer must be foreseen in the experimental apparatus. The permeation regime can be evaluated by means of the permeation parameter W_Q [11], which in case of multiple isotopes permeation (hydrogen and tritium for this application) can be expressed as [12]:

$$W_Q = \frac{k_r k_S}{D_T} \cdot t_s \cdot \sqrt{p_T + p_H} \tag{1}$$

where k_r (m^4 mol^{-1} s^{-1}), k_S (mol m^{-3} $Pa^{-1/2}$) and D_Q (m^2 s^{-1}) are the recombination constant, Sieverts' constant and diffusion coefficient of tritium through the membrane, t_s (m) is the membrane thickness, $p_T = p_{T_2} + 0.5p_{HT}$ and $p_H = p_{H_2} + 0.5p_{HT}$ (Pa) are the effective pressures of tritium and hydrogen at the high-pressure side of the membrane, respectively. Basically, if $W_Q \gg 1$, the permeation regime is diffusion-limited, if $W_Q \ll 1$ the regime is surface-limited; the mixed regime is characterized by $W_Q \approx 1$. The term *limited* is referred to the slowest process which governs the system. In particular, in a surface-limited regime, the surface reactions of dissociation and recombination governs the net flow of molecules through the membrane.

In equilibrium mode, starting from vacuum conditions, there is an increase in pressure inside the volume of the sensor due to the flow of hydrogen isotopes permeated through its walls. The pressure inside the measuring head changes until its value is equal to the partial pressure of hydrogen solubilized in sodium. Once this value is measured by the pressure transducer, it is possible to derive the concentration of hydrogen isotopes solubilized in the liquid phase through the Sieverts' law:

$$c_{Q,l} = k_{S,l} \cdot \sqrt{p_{eq,Q_2}} \tag{2}$$

where $c_{Q,l}$ (mol m^{-3}) is the hydrogen isotopes concentration in liquid sodium and $k_{S,l}$ (mol m^{-3} $Pa^{-1/2}$) is the Sieverts' constant of Q species in liquid sodium; it has to be observed that the hydrogen isotope is dissolved in its monatomic form in the liquid metal, whereas in gas phase it is found in diatomic form. The results provided in the equilibrium mode operation are influenced mainly by the accuracy on Sieverts' constant. Only the pressurization time of the capsule is influenced by the rate of permeation, not the final pressure, which is the only measurement required. The time taken by the sensor to attain the equilibrium pressure should be as short as possible, for an efficient operational measurement of the concentration.

In dynamic mode, a measurement of the permeation flux, J_p (mol m^{-2} s^{-1}), is assessed by the quadrupole mass spectrometer. The permeation flux depends on the membrane characteristics, i.e. diffusivity, Sieverts' constant and surface parameters of the material [12, 13].

As detailed in [5], a 2D axial-symmetric hydrogen isotopes transport code (HIT) was developed through COMSOL Multiphysics [14] in order to solve a mixed permeation regime for fusion applications but can be extended to fission. The HIT code solves, both in the gas or liquid metal domain and in the membrane domain, a passive, scalar, general transport equation:

$$\frac{\partial c}{\partial t} + \vec{u} \cdot \nabla c + \nabla \cdot (-D \nabla c) = 0 \tag{3a}$$

$$\vec{J}_d = -D \nabla c + c\vec{u} \tag{3b}$$

where c (mol m^{-3}) is the hydrogen isotope concentration, $\vec{u}$ (m s^{-1}) is the velocity field, D (m^2 s^{-1}) is the diffusion coefficient, s (mol m^{-3} s^{-1}) is the source term and $\vec{J}_d$ (mol m^{-2} s^{-1}) is the transport flux. For the present application, the convective term related to the velocity field of the gas and the source term were assumed equal to zero. At the interface sodium/membrane, pressure continuity was assumed, i.e. continuity of the chemical potential, leading to the discontinuity of concentration at the interfaces:

$$\frac{c|_{\partial\Omega_{m,Na}}}{c|_{\partial\Omega_{Na,m}}} = K_{LP} \tag{4}$$

where $c|_{\partial\Omega_{m,Na}}$ is the Q concentration evaluated at the membrane/sodium interface, $c|_{\partial\Omega_{Na,m}}$ is the concentration evaluated at the sodium/membrane interface, $K_{LP} = k_S/k_{S,Na}$ is called partition coefficient and expresses the ratio between the Sieverts' constant of the membrane with respect to the Sieverts' constant of liquid sodium. Furthermore, also the flux continuity must be ensured at the sodium/membrane interface:

$$\vec{J}_d|_{\partial\Omega_{m,Na}} = \vec{J}_d|_{\partial\Omega_{Na,m}} \tag{5}$$

On the other hand, the net flow of hydrogen isotopes atoms through the membrane/vacuum interface could be written as:

$$\vec{J}_Q = k_r c_Q^2 - k_d p_{Q_2} \quad \text{at } \partial\Omega|_{V,m} \tag{6}$$

$$\vec{J}_{Q_2} = -2J_Q \quad \text{at } \partial\Omega|_{m,V} \tag{7}$$

where k_r (m^4 mol^{-1} s^{-1}) is the recombination constant and k_d (mol m^{-2} s^{-1} Pa^{-1}) is the dissociation constant. Eq. (7) is evaluated at the vacuum/membrane interface, whereas Eq. (8) at the membrane/vacuum interface. The factor 2 takes into account that tritium is solubilised monoatomically in the metal, while it assumes a molecular form in gas phase. A schematic representation of the processes involved is displayed in Figure 2.

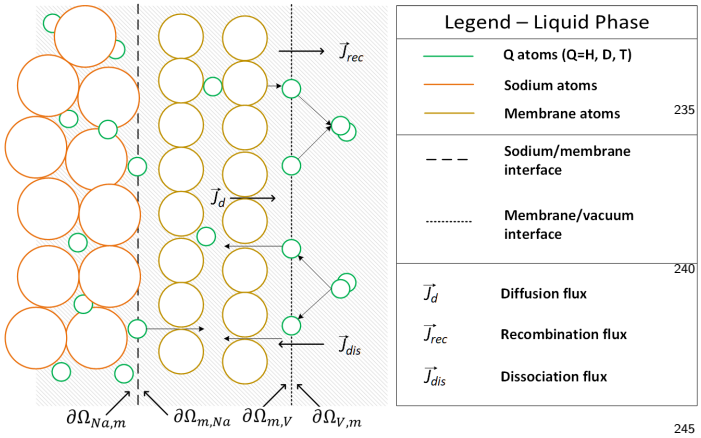

Figure 2: Representation of permeation phenomena for liquid phase model.

3. Design of the measuring head

3.1. Choice of the materials

The assessment of the design of a hydrogen/tritium meter for the primary and secondary circuit of a sodium fast reactor was carried out on the basis of a) the main chemical-physical and transport properties of sodium, b) the transport properties (solubility, diffusivity, permeability) of hydrogen in different metals and alloys, c) the chemical compatibility of materials in liquid sodium from the viewpoint of corrosion and oxidation. As far as the first point is concerned, chemical-physical properties were taken from NAPRO database for liquid sodium [15]; the Sieverts' constant of hydrogen was derived from the Whittingham correlation for solubility [16] and from the equilibrium pressure equation [17]. This results in:

$$\log k_{S,W}(\text{wppm Pa}^{-1/2}) = -0.318 - \frac{60.5}{T(K)} \qquad (8)$$

where the subscript W stands for Whittingham. Measurements with tritium have not been performed yet. However, *Veleckis et al.* [18] studied the LiH, LiD and LiT systems and showed that the decomposition pressures for equal gas concentration in sodium are related through the following relationship: $p_{T_2} > p_{D_2} > p_{H_2}$, where $p_{T_2}/p_{H_2} = 3^{1/2}$ and $p_{D_2}/p_{H_2} = 2^{1/2}$. They conclude that, considering solubilities, there is no influence of the isotopic form of the hydrogen element providing the gas pressures are correlated as reported above. Concerning Sieverts' constant, since $k_{S,Q} = c_{Q,l} \cdot p_{Q_2}^{1/2}$, one can write:

$$\log k_{S,T} = 3^{-1/4} \cdot k_{S,H} = 0.76 \cdot k_{S,H} \qquad (9)$$

where $k_{S,H}$ is the Sieverts' constant of hydrogen evaluated by means of Equation 8 and $k_{S,T}$ is the Sieverts' constant for tritium. This assumption is in agreement with that used in [19] for the development of tritium transport models for SFRs.

From the point of view of transport properties of the membrane (permeability, diffusivity, Sieverts' constant and recombination constant), several materials were considered. Among these, nickel, tantalum, niobium, titanium and vanadium were selected on the basis of the chemical compatibility with liquid sodium, as shown in Table 2. The values of k_r were taken from the experimental results reported in [20, 21]. It should be pointed out that the calculation of the recombination constant was also performed with Baskes [22] and Pick and Sonnenberg [20] theoretical models, but the values were in contrast with those from experiments, with differences up to several orders of magnitude. This inconsistency can be attributed to the fact that theoretical models does not include surface imperfections, chemisorption impurity atoms, etc.

From the point of view of chemical compatibility, the main results referring to Gibbs free energy for oxides formation ΔG_f^0 (kJ mol^{-1}), oxidation weight gain w (mg cm^{-2}) and corrosion weight loss in sodium k (mg cm^{-2} y^{-1}) are reported in Table 3. The oxides considered were NiO, Ta_2O_5, Nb_2O_5, TiO_2, V_2O_5 which are the most common oxides formed by the respective pure metals [23, 24, 25, 26, 27]. The Gibbs free energy was evaluated according to [23] at 450 °C and reported per unit mole of oxygen. The corrosion rates of different pure elements in liquid sodium were deeply investigated in [17, 28, 29, 30, 31]. In particular, the corrosion of nickel in sodium has been investigated as a function of temperature and velocity in a sodium loop; moreover, exposure of nickel specimens has been performed in the EBR-II reactor [32]. The weight loss was linear with time, whereas the impact of neutron fluence was negligible. Tantalum is very resistant to sodium exposure with a weight loss varying from 0.9 to 11.1 [mg cm^{-2} y^{-1}] at 430 °C and 10 wppm oxygen [29]. The weight gain was evaluated after one-hour exposure in the temperature range 400-500 °C and at an oxygen pressure of 1 atm [24, 33, 34].

Based on the above three points, nickel and tantalum were preliminarily selected as candidate materials. Nickel, in particular, is characterized by low Gibbs free energy of oxidation and is weakly reactive with liquid sodium; however, it presents lower value of permeability and diffusivity with respect to tantalum. On the other hand, tantalum is more reactive with oxygen, it has a higher permeability and diffusivity, therefore presenting a higher Sieverts' constant. For the application to the laboratory set-up, nickel

Table 2: Permeability, diffusivity, Sieverts' constant and recombination constant for hydrogen in Ni, Ta, Nb, Ti and Va at 450 °C.

Material	P_m (mol m^{-1} s^{-1} Pa$^{-0.5}$)	D_m (m^2 s^{-1})	$k_{S,m}$ (mol m^{-3} Pa$^{-0.5}$)	$k_{r,m}$ (m^4 mol^{-1} s^{-1})
Nickel	$1.077 \cdot 10^{-11}$	$9.397 \cdot 10^{-10}$	$1.147 \cdot 10^{-2}$	$1.2 \cdot 10^{-5}$
Tantalum	$1.670 \cdot 10^{-7}$	$4.485 \cdot 10^{-8}$	3.724	$1.147 \cdot 10^{-8}$
Niobium	$4.046 \cdot 10^{-7}$	$5.234 \cdot 10^{-9}$	77.3	$1.5 \cdot 10^{-8}$
Titanium	$7.051 \cdot 10^{-7}$	$4.784 \cdot 10^{-10}$	1474	$6.0 \cdot 10^{-12}$
Vanadium	$2.499 \cdot 10^{-7}$	$4.474 \cdot 10^{-9}$	55.9	$1.5 \cdot 10^{-8}$

Table 3: Gibbs free energy and oxidation kinetics and corrosion for Ni, Ta, Nb, Ti and Va.

Material	ΔG_f^0 (kJ mol^{-1})	w (μg cm^{-2})	k (mg cm^{-2} y^{-1})
Nickel	-173	20	0.3
Tantalum	-689	0-40	0.9-11.1
Niobium	-632	8000	26.4
Titanium	-811	6	14-84
Vanadium	-495	21	164

was chosen as candidate material; as far as the application to SFR is concerned, tantalum is foreseen.

Furthermore, the permeation parameter was calculated according to the pressure range of the conceptual SFR, leading to $5.1 \cdot 10^{-5}$. It followed that the permeation regime is always surface-limited, even if the partial pressure of hydrogen isotopes was 1 Pa (value referred to the nickel membrane). For tantalum, the permeation parameter at the operative conditions foreseen for SFRs would be 0.1.

3.2. Simulations of sensor behaviour

Several numerical simulations of multiple-isotopes permeation [12] were carried out. In this way, the sensor behaviour was described in equilibrium mode and in dynamic mode, and the preliminary sensor design was optimized. The main input data are reported in Table 4.

Table 4: Input parameters for modelling simulations.

Parameter	Value	Units.
S/V ratio, S_V	$100 - 5000$	m^{-1}
Membrane thickness, t_s	$2 \cdot 10^{-4}$	m
Internal diameter, d_{in}	$1.93 \cdot 10^{-3}$	m
H_2 partial pressure, p_{H_2}	$7.65 \cdot 10^{-3}$	Pa
T_2 partial pressure, p_{T_2}	$4.68 \cdot 10^{-6}$	Pa
Op. temperature, T_{op}	$400, 450, 500$	°C
Vacuum pressure p_0	$1 \cdot 10^{-8}$	Pa
Sieverts' constant H	0.669	wppm Pa$^{-0.5}$
Sieverts' constant T	0.509	wppm Pa$^{-0.5}$

The S/V ratio is the ratio of the external surface area to the empty volume of the cylinder and for a cylinder can be evaluated as:

$$S_V = 4\frac{d_{in} + 2t_s}{d_{in}^2} \tag{10}$$

A first attempt of calculation was performed assuming a membrane thickness equal to $2 \cdot 10^{-4}$ m and an internal diameter of $1.93 \cdot 10^{-3}$ m in order to have S_V=2500. According to [4], a helical-shaped sensor was selected as reference geometry since it maximizes the ratio of exposed surface to space needed for the sensor, and minimizes the internal volume of the sensor and minimizes the number of weldings to be made. In equilibrium mode, the pressure rise in the internal chamber of the sensor is reported in Figure 3. The vacuum pressure was set to 10^{-8} Pa to ensure the hydrogen isotopes permeation. Considering the tantalum membrane, the response time, evaluated as the time necessary to reach the 90% of the asymptotical value of the pressure, is reduced by 46% and 29% with respect to nickel for H_2 and T_2, respectively (Table 5).

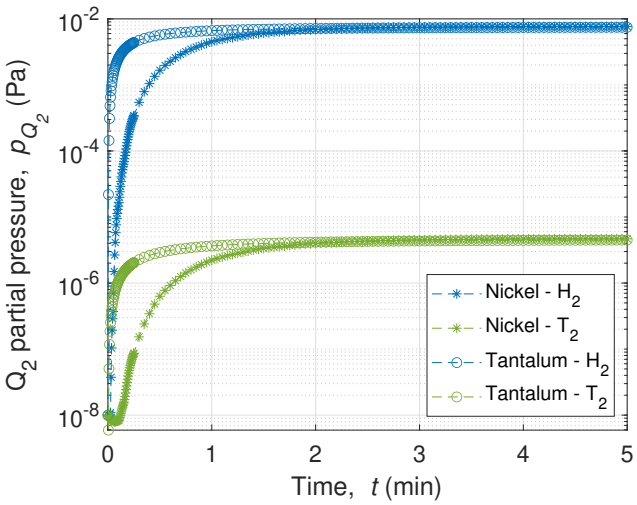

Figure 3: Pressure rise in the internal chamber of HPS for two-species permeation, Ni and Ta membranes; $p_{H_2} = 7.65 \cdot 10^{-3}$ Pa, $p_{T_2} = 4.60 \cdot 10^{-6}$ Pa, $T = 450$ °C.

The response time for hydrogen was plotted as a function of the S_V ratio as displayed in Figure 4 in the case of the Ta membrane. It can be noted that the response time shows a decreasing asymptotic behaviour for $S_V \to \infty$. This means, that increasing too much the S_V ratio does

Table 5: Response time for Ni and Ta membranes, equilibrium mode.

	Response time, $t_{90\%}$ (s)	
	Ta membrane	Ni membrane
Hydrogen	63	117
Tritium	96	135

not change the equilibrium response time. This time is the minimum response time value that can be achievable.

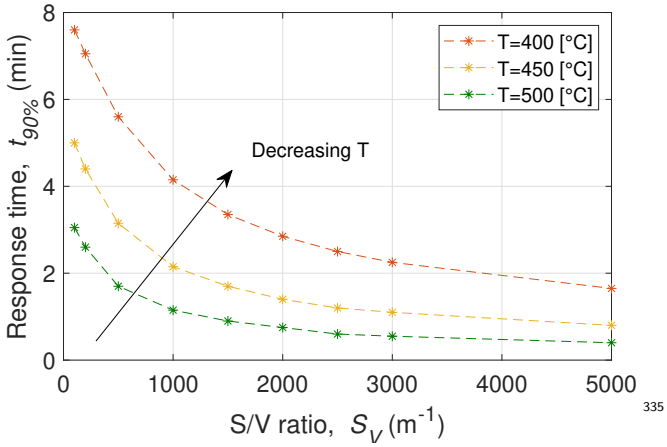

Figure 4: Response time as a function of S/V ratio, Ta membrane.

In dynamic mode (Table 6), the response time is much lower than that in equilibrium mode. In addition, in the case of the tantalum membrane, the response time for hydrogen and tritium is reduced by 63% and 66%, respectively, with respect to nickel. The asymptotic value of the permeation flux is in general two orders of magnitude higher for tantalum, as detailed in Table 6. In order to have a dynamic fast response of the sensor, the HPS for sodium applications has to be operated in dynamic mode.

Table 6: Response time and steady-state flux for Ni and Ta membranes, dynamic mode.

	Response time, $t_{90\%}$ (s)	
	Ta membrane	Ni membrane
Hydrogen	9	24
Tritium	14	42
	Steady-state permeation flux, J_p (mol m^{-2} s^{-1})	
Hydrogen	$7.757 \cdot 10^{-10}$	$6.033 \cdot 10^{-12}$
Tritium	$8.062 \cdot 10^{-13}$	$6.385 \cdot 10^{-15}$

3.3. Final design of the measuring head

According to tube manufacturers, the most suitable solution is constituted by $2 \cdot 10^{-3}$ m external diameter and

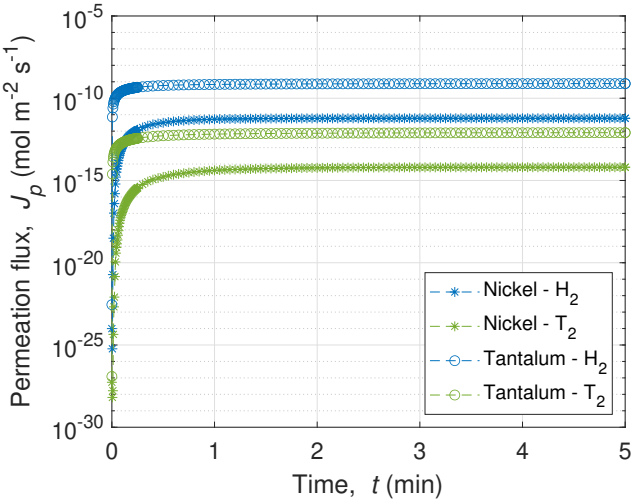

Figure 5: Permeation flux in dynamic mode, Ni and Ta membranes; $p_{H_2} = 7.65 \cdot 10^{-3}$ Pa, $p_{T_2} = 4.60 \cdot 10^{-6}$ Pa, $T = 450$ °C.

$2 \cdot 10^{-4}$ m thickness pipe. In this case, the S/V ratio is equal to 3125 m^{-1}, but this has not a remarkable impact on the performances analysed in the previous paragraph as highlighted in Figure 4. A drawing of the permeation sensor is displayed in Figure 6. The sensor is welded to a 1/4" Swagelok connection pipe and it is characterized by only two weldings, a butt weld at the end of the helix and an orbital weld between the sensor itself and the connection pipe. Welding can be performed by a standard GTAW technique, preferably in an inert gas chamber to minimize interactions with oxygen. The main design characteristics are given in Table 7. A discussion on the proposed design and on the possible upgrades are given in Chapter 4.1.

Table 7: Geometrical parameters of Ni permeation sensor.

Parameter	Value
Minor diameter, d	$2 \cdot 10^{-3}$ m
Major diameter, D	$2.6 \cdot 10^{-2}$ m
Pitch between coils, p	$5 \cdot 10^{-3}$ m
Height of the sensor, H	$6 \cdot 10^{-2}$ m
Thickness, t_s	$2 \cdot 10^{-4}$ m
Angle between coils, α	3.8°
Number of coils, N	8
Total tube length, l_{tot}	$6.3 \cdot 10^{-1}$ m

3.4. Tritium measurement and memory effect

The hydrogen/tritium permeation sensor with tantalum membrane for a SFR needs to be integrated with a mass spectrometer or a ionization chamber. The proposed design adopts a quadrupole mass spectrometer as a tool to measure the individual components in the gas stream. The gas is introduced at low pressure into a chamber and

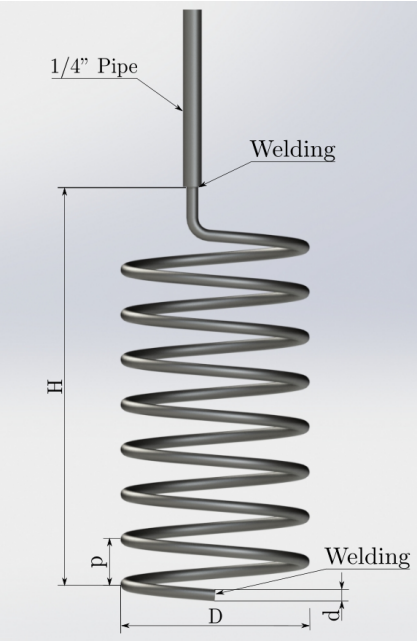

Figure 6: Drawing of hydrogen isotopes permeation sensor.

ionized. The ions produced are then measured by a system that discriminates the different masses. The number of ions produced at each mass is measured and is proportional to the partial pressure of the component in the gas sample. Due to the radioactivity of the tritium, particular attention is required in the use of mass spectrometry for the analysis of tritium containing gas. Moreover, the mass spectrometer proposed in the design is equipped with a triple mass filter which is able to reduce the noise level; the retention of tritium can be easily reduced by outgassing the filament.

Ionization chambers are generally used to monitor the tritium level in a gas stream because of their reliability, flexibility and wide range of measurement. However, they are subject to the memory effect. The memory effect is mainly due to the adsorption of tritium onto the electrodes of the ionization chamber; it is well-known that this effect can reduce the accuracy of the measurements. To reduce this effect, several solutions are proposed. For instance, swamping with water vapor can diminish the memory effect to background level after about 30 minutes, due to the promoting desorption of tritium by means of the reaction between tritiated water in surface water on the electrode material (usually copper) and water vapor in the gas stream [35]. Recent experiments with tritium in form of both HTO and HT were carried out at the Institute of Nuclear Physics and Chemistry (INCP) to examine the effect of memory effect and results showed that a gold plated treatment of the internal part of the chamber could effectively reduce the influence of memory effect caused by tritium absorption to background level in 1 minute after 1 h of tritium exposure with dry air swamping [32].

Another technology which can be adopted for the monitoring of tritiated gas species is the Beta-induced X-ray spectrometry (BIXS) [36]. This method is based on the measurement of bremsstrahlung radiation and characteristic X-rays generated by interactions of beta particles with the surfaces inside the measurement chamber. Even in this case, the accuracy is limited by the memory effect due do the absorption of tritium onto the surfaces. Recent studies [37] showed that the lowest memory effect can be achieved by means of gold-coated cells. It was found that the tritium-induced background level of uncoated stainless steel 316 LN was on the same level. Other materials, such as multi-layer systems with a gold coating or ceramics, have been found to yield sufficient memory reduction. A comprehensive review of the most adopted technologies for tritium measurement can be found in [38]. Ioniziation chambers and BIXS will be analyzed in detail as a future step of this work.

4. Design of the full sensor line

In order to operate the measuring head, it is necessary to realize a vacuum system and a gas line. The Process Flow Diagram (PFD) of the full sensor assembly is reported in Fig. 7.

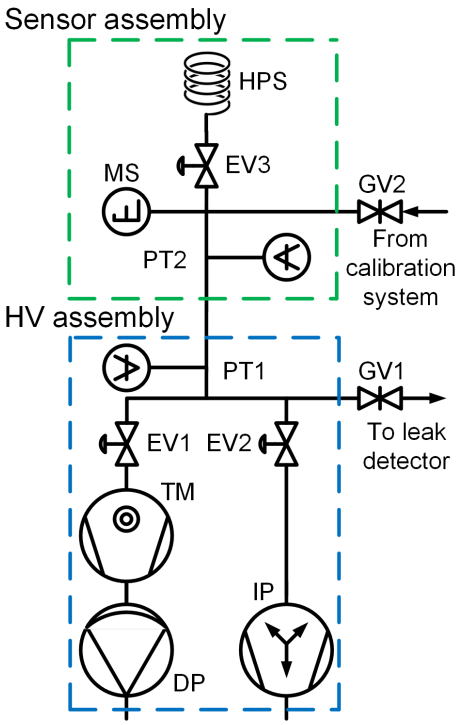

Figure 7: PFD of the sensor line. IP: ion pump; DP: diaphragm pump; TM: turbomolecular pump; PT: pressure transducer; MS: quadrupole mass spectrometer; HPS: hydrogen isotopes permeation sensor; GV: manual gate valve; EV: electropneumatic gate valve.

The main assemblies are described as follows. The high vacuum system (HV assembly) consists of a backing

pumping station constituted by a diaphragm pump (DP) and a turbomolecular pump (TM). This system allows to reach the backing pressure of the ion pump (IP), indicatively $1 \cdot 10^{-3} - 1 \cdot 10^{-2}$ Pa. The pressure is read by a Pirani/Bayard-Alpert vacuum gauge, PT1. The IP pump is used to reach HV conditions. Due to the presence of mainly hydrogen (and outgassing from piping) and for the range of vacuum pressure to be addressed, an ion pump is identified as the preferred candidate. The HV assembly interfaces with the sensor assembly, with the leak detection system and the venting system. The leak detection system is connected to the HV assembly by means of a dedicated line.

The sensor assembly line directly interfaces with the HPS permeation sensor submerged in the liquid sodium. The connection from the sensor to the mass spectrometer (MS) is characterized by a 1/4" Swagelok pipe. A possible choice for the mass spectrometer could be a triple filter model, which allows to reduce the signal noises and is characterized by increased mass resolution. A Bayard-Alpert gauge (BA) or an extractor system gauge (ES), labelled as PT2, is used to have a double-check on the pressure reading with respect to PT1. This system interfaces also with the calibration system, to be used for the calibration of the mass spectrometer.

Regarding the materials of the vacuum lines, austenitic steels, for example AISI 304L or AISI 316LN, are the main candidates, being widely used in HV/UHV systems. Type 300 stainless steels presents good overall compatibility in the vacuum environment and can be baked at several hundreds of degrees or vacuum fired at around 1000 °C [39]. Finally, the effective pumping speed of the ion pump at the level of the vacuum instruments was evaluated as $S_{eff} \approx C_{tot} = 5.5$ l s^{-1}.

4.1. Discussion on the proposed design

The main source of hydrogen outgassing from the system described in Figure 7 is principally due to the pressure transducer PT2 and the quadrupole mass spectrometer MS. The total outgassing rate from these two instruments can be assumed equal to $\sim 10^{-5}$ Pa m s^{-1}. Considering an effective pumping speed $S_{eff} \approx C_{tot}$, it comes out that the pressure limit due to the only presence of instruments is $2 \cdot 10^{-7}$ Pa. In addition to the instrumentation contribution on the final pressure of the system, the hydrogen outgassing from the pipes was evaluated. Considering an outgassing rate $q_{des} = 1 \cdot 10^{-9}$ Pa m s^{-1} [40], the contribution due to the piping system was calculated as $2.4 \cdot 10^{-8}$ Pa. On the other hand, assuming the asymptotic value of the hydrogen permeation flux shown in Fig. 5, the contribution of the permeating hydrogen is $2.6 \cdot 10^{-8}$ Pa. Therefore, the total contribution to the pressure limit due to instrumentation and pipelines is one order of magnitude higher than that of permeating hydrogen. The actual design with the nickel membrane is able to detect hydrogen partial pressures higher than 0.1 Pa and will be adopted in the laboratory test section in the range 1-10 Pa. However, this kind of sensor would be able to measure HT or T_2, since the background of the mass spectrometer in the range 4-6 amu is in general very low.

Regarding the tantalum membrane, the design proposed would result in a contribution due to the permeating hydrogen equal to $3.4 \cdot 10^{-6}$ Pa, i.e. one order of magnitude higher with respect to the total contribution due to piping and instrumentation. It should be observed that this value can be increased to $1.6 \cdot 10^{-5}$ Pa if the sensor would be characterized by $d = 5.9 \cdot 10^{-3}$ m, $t_s = 1.25 \cdot 10^{-4}$ m, $L = 1$ m, which is two orders of magnitude higher with respect to the total piping and instrumentation contribution. In case of the Ta membrane, the requirements for a conceptual SFR reported in Table 1 are satisfactorily met. Concerning the tritium partial pressure, the reliability of the HPS relies on the resolution of the quadrupole mass spectrometer, for which a triple filter model was suggested.

5. Conclusions

A new hydrogen isotopes permeation sensor and its integration into a HV system was presented. The measuring head was designed on the basis of the HIT code used for the development of hydrogen permeation sensors for fusion applications and adapted to fission, taking advantage of the experience gained with LiPb laboratory. The most suitable materials appeared to be nickel and tantalum. Nickel, in particular, is characterized by low Gibbs free energy of oxidation and is weakly reactive with liquid sodium; however, it presents lower value of permeability and diffusivity with respect to tantalum. On the other hand, tantalum is more reactive with sodium, it has a higher permeability and diffusivity but presents a higher Sieverts' constant. This means that tantalum traps a higher quantity of hydrogen isotopes in the bulk. For the application to the laboratory set-up, nickel was chosen as candidate material due to the necessity for the facility to be operated at pressure in the range 1-10 Pa; as far as the application to SFR is concerned, where lower pressure measurements are required, tantalum was selected.

The instrumentation and the components necessary to operate the assembly were accurately selected on the basis of the requirements of a SFR. The vacuum is generated through a sputter-ion pump, for which the rough vacuum is realized by means of a combined diaphragm/turbomolecular pumping station. A double check on the pressure inside the line has been proposed by adopting two different pressure transducers: the Pirani/Bayard-Alpert monitors the pressure evolution from atmospheric pressure to HV conditions, whereas a hot cathode or extractor gauge will be used in HV conditions in order to have a more accurate pressure reading and higher repeatability. A possible choice for the mass spectrometer could be a triple filter model, which allows to reduce the signal noises and is characterized by increased mass resolution. The vacuum valves

for the normal operation of the assembly are electropneumatic with position indicator.

Finally, the two different designs proposed were discussed. The nickel membrane cannot be adopted in a sodium fission reactor due to the fact that the pressure limit due to the pipelines and instrumentation is higher than the pressure due to the permeating hydrogen, although for the tritium point of view it could be measured due to the low background in correspondence of 4-6 amu. To increase the permeation flux and consequently to increase the contribution of permeating hydrogen, a tantalum membrane can be adopted. The sensitivity on tritium partial pressure relies on the resolution of the mass spectrometer. In this way, the requirements on the very low partial pressure for Q_2 species which can be found in the liquid sodium of a SFR are satisfactorily met.

Acknowledgments

This research did not receive any specific grant from funding agencies in the public, commercial, or not-for-profit sectors. We would like to thank Dr. Thierry Gilardi (CEA Cadarache, France) for providing useful discussions on tritium topics related to sodium fast reactors and for his assistance at the different stages of this research.

References

[1] K. Korsah, R.A. Kisner, C.L. Britton Jr., Pradeep Ramuhalli, D. W. Wootan, N.C. Anheier Jr., A. A. Diaz, E. H. Hirt, R. B. Vilim, H. T. Chien, S. Bakhtiari, S. Sheen, S. Gopalsami, A. Heifetz, S.W. Tam, Y. Park, B. R. Upadhyaya, Austin Stanford, UTK, Sensor technology assessment for advanced reactors, Advanced Sensors and Instrumentation 2016 NE I&C Review (Oak Ridgen National Laboratory, October 12-12, 2016).

[2] A. Ciampichetti, M. Zucchetti, I. Ricapito, M. Utili, A. Aiello, G. Benamati, Performance of a hydrogen sensor in Pb–16Li, Journal of Nuclear Materials 367-370 (2007) 1090–1095, proceedings of the Twelfth International Conference on Fusion Reactor Materials (ICFRM-12). doi:https://doi.org/10.1016/j.jnucmat.2007.03.250.

[3] I. Nicolotti, M. Utili, L. Candido, M. Zucchetti, A hydrogen sensor for liquid-metal breeding blankets, Transactions of the American Nuclear Society 112 (2015) 193–196, 2015 ANS Annual Meeting, San Antonio, TX.

[4] L. Candido, I. Nicolotti, M. Utili, M. Zucchetti, Design optimization of a hydrogen sensor for ITER Pb16Li blankets, IEEE Transactions on Plasma Science 45 (7) (2017) 1831–1836. doi:10.1109/TPS.2017.2710218.

[5] L. Candido, M. Cantore, E. Galli, R. Testoni, M. Zucchetti, M. Utili, A. Ciampichetti, Characterization of Pb-15.7Li hydrogen isotopes permeation sensors and upgrade of HyPer-Quarch experimental device, IEEE Transactions on Plasma Science 48 (6) (2020) 1505–1511. doi:10.1109/TPS.2020.2974937.

[6] I. Ricapito, A. Aiello, A. Bükki-Deme, J. Galabert, C. Moreno, Y. Poitevin, D. Radloff, A. Rueda, A. Tincani, M. Utili, Tritium technologies and transport modelling: main outcomes from the European TBM project, Fusion Engineering and Design 136 (2018) 128–134, special Issue: Proceedings of the 13th International Symposium on Fusion Nuclear Technology (ISFNT-13). doi:https://doi.org/10.1016/j.fusengdes.2018.01.023.

[7] K. Korsah, R. A. Kisner, C. L. Britton, P. Ramuhalli, D. W. Wootan, N. C. Anheier, A. A. Diaz, E. H. Hirt, R. B. Vilim, H. T. Chien, et al., Sensor technology assessment for advanced reactors, Tech. Rep. ORNL/TM-2016/337 R1, Oak Ridge National Laboratory (2017). doi:10.2172/1345781.

[8] M. Sturm, M. Schlösser, R. J. Lewis, et al., Monitoring of all hydrogen isotopologues at tritium laboratory Karlsruhe using Raman spectroscopy, Laser Physics 20 (2010) 493–507. doi:https://doi.org/10.1134/S1054660X10030163.

[9] M. Schlösser, S. Rupp, H. Seitz, S. Fischer, B. Bornschein, T. M. James, H. H. Telle, Accurate calibration of the laser raman system for the karlsruhe tritium neutrino experiment, Journal of Molecular Structure 1044 (2013) 61–66. doi:https://doi.org/10.1016/j.molstruc.2012.11.022.

[10] T. B. Cochran, H. A. Feiveson, W. Patterson, G. Pshakin, M.V. Ramana, M. Schneider, T. Suzuki, F. von Hippel, Sensor technology assessment for advanced reactors, Tech. Rep. Vol. 8, International Panel on Fissile Materials (2010).

[11] I. Ali-Khan, K.J. Dietz, F.G. Waelbroeck, P.Wienhold, The rate of hydrogen release out of clean metallic surfaces, Journal of Nuclear Materials 76-77 (1978) 337–343. doi:https://doi.org/10.1016/0022-3115(78)90167-8.

[12] P. W. Humrickhouse, Permeation of multiple isotopes in the transition between surface and diffusion-limited regimes, Tritium Focus Group meeting (Idaho National Laboratory, 2014).

[13] O. Richardson, J. Nicol, T. Parnell, I. the diffusion of hydrogen through hot platinum, The London, Edinburgh, and Dublin Philosophical Magazine and Journal of Science 8 (43) (1904) 1–29. doi:https://doi.org/10.1080/14786440409463168.

[14] COMSOL Multiphhysics, v. 5.6, http://www.comsol.com/, Accessed: 2021-01-31.

[15] O. Azpitarte, M. Japas, M. Chocrón, E. Vázquez, A. Villanueva, The iaea coordinated research project on sodium properties and safe operation of experimental facilities in support of the development and deployment of sodium-cooled fast reactors (napro), Tech. rep., IAEA (2017).

[16] A. Whittingham, An equilibrium and kinetic study of the liquid sodium-hydrogen reaction and its relevance to sodium-water leak detection in lmfbr systems, Journal of Nuclear Materials 60 (2) (1976) 119–131. doi:https://doi.org/10.1016/0022-3115(76)90157-4.

[17] H. U. Borgstedt, C. Guminski, H. U. Borgstedt, C. Guminski, Iupac-nist solubility data series. 75. nonmetals in liquid alkali metals, Journal of Physical and Chemical Reference Data 30 (4) (2001) 835–1158. doi:https://doi.org/10.1063/1.1391426.

[18] E. Veleckis, R. K. Edwards, Thermodynamics properties in the systems vanadium-hydrogen, niobium-hydrogen, and tantalum-hydrogen, Journal of Physical Chemistry 73 (1969) 683–692.

[19] T. A. Ranner, C. C. McPheeters, Tritium and hydrogen transport in lmfbr systems: Ebr- ii, crbr, and fftf, Tech. Rep. ANL-78-64, Argonne National Laboratory (1978).

[20] M. Pick, K. Sonnenberg, A model for atomic hydrogen-metal interactions — application to recycling, recombination and permeation, Journal of Nuclear Materials 131 (2) (1985) 208–220. doi:https://doi.org/10.1016/0022-3115(85)90459-3.

[21] A. Pisarev, K. Miyasaka, T. Tanabe, Permeation of hydrogen through tantalum: influence of surface effects, Journal of Nuclear Materials 317 (2) (2003) 195–203. doi:https://doi.org/10.1016/S0022-3115(03)00079-5.

[22] M. Baskes, A calculation of the surface recombination rate constant for hydrogen isotopes on metals, Journal of Nuclear Materials 92 (2) (1980) 318–324. doi:https://doi.org/10.1016/0022-3115(80)90117-8.

[23] I. Barin, Thermochemical Data of Pure Substances, Third Edition, 3rd Edition, John Wiley & Sons, Ltd, 1995, an optional note. doi:https://doi.org/10.1002/9783527619825.

[24] J. E. J.M Perrow, W.W Smeltzer, The role of structural defects in the growth of nickel oxide films, Acta Metallurgica 16 (10) (1968) 1209–1218. doi:https://doi.org/10.1016/0001-6160(68)90002-3.

[25] S. P. Garg, N. Krishnamurthy, A. Awasthi, M. Venkatraman, The o-ta (oxygen-tantalum) system, Journal of Phase Equilibria 17 (1) (1996) 63–77. doi:https://doi.org/10.1007/BF02648373.

[26] J. S. Sheasby, The oxidation of niobium in the temperature range 450°–720°c, Journal of the Electrochemical Society 115 (7) (1996) 695–700. doi:https://doi.org/10.1149/1.2411404.

[27] A. J. Bergerud, Phase stability and transformations in vanadium oxide nanocrystals, Ph.D. thesis, University of California, Berkeley (2016).

[28] C. F. Cheng, W. E. Ruther, Corrosion of Nickel in Liquid Sodium, Corrosion 28 (1) (1972) 20–22. doi:https://doi.org/10.5006/0010-9312-28.1.20.

[29] G. E. Raines, C. V. Weaver, J. H. Stang, Corrosion and creep behavior of tantalum in flowing sodium, Tech. Rep. BMI-1284, Battelle Memorial Inst., Columbus, Ohio (8 1958). doi:https://doi.org/10.2172/4299756.

[30] A. W. Thorley, J. A. Bardsley, Structural changes in materials exposed to liquid sodium, Journal of the Royal Microscopical Society 88 (4) (1968) 431–447. doi:https://doi.org/10.1111/j.1365-2818.1968.tb00625.x.

[31] R. L. Ammon, Vanadium and vanadium-alloy compatibility behaviour with lithium and sodium at elevated temperatures, International Metals Reviews 25 (1) (1980) 255–268. doi:https://doi.org/10.1179/imtr.1980.25.1.255.

[32] Z. Chen, S. Peng, P. Chen, R. Chang, G. Wu, Y. Li, Improvement of ionization chamber for tritium measurements in in-pile tritium extraction experiments, Fusion Engineering and Design 147 (2019) 111222. doi:https://doi.org/10.1016/j.fusengdes.2019.05.041.

[33] V. B. Voitovich, V. A. Lavrenko, V. M. Adejev, E. I. Golovko, High-temperature oxidation of tantalum of different purity, Oxidation of Metals 43 (5-6) (1995) 509–526.

[34] R. Haugsrud, On the high-temperature oxidation of nickel, Corrosion Science 45 (2003) 211–235.

[35] M. Nishikawa, T. Takeishi, Y. Matsumoto, I. Kumabe, Ionization chamber system to eliminate the memory effect of tritium, Nuclear Instruments and Methods in Physics Research Section A: Accelerators, Spectrometers, Detectors and Associated Equipment 278 (2) (1989) 525–531. doi:https://doi.org/10.1016/0168-9002(89)90875-9.

[36] M. Matsuyama, K. Watanabe, K. Hasegawa, Tritium assay in materials by the bremsstrahlung counting method, Fusion Engineering and Design 39-40 (1998) 929–936. doi:https://doi.org/10.1016/S0920-3796(98)00232-4.

[37] M. Aker, M. Röllig, Material studies to reduce the tritium memory effect in bixs analytic systems, Fusion Science and Technology 76 (3) (2020) 373–378. doi:https://doi.org/10.1080/15361055.2020.1712989.

[38] P. Fichet, A. Bultel, S. Markelij, C. Moreno, Review of the different techniques to analyse tritium, Tech. Rep. WP02-D2.1, CEA, France (7 2018).

[39] R. Calder, G. Lewin, Reduction of stainless-steel outgassing in ultra-high vacuum, British Journal of Applied Physics 18 (1967) 1459–1472.

[40] P. Chiggiato, Outgassing properties of vacuum materials for particle accelerators, Proceedings of the 2017 CERN-Accelerator-School course on Vacuum for Particle Accelerators, Glumslöv, (Sweden) (2017) 1–43.